J Solid State Electrochem (2001) 6: 1–7
DOI 10.1007/s100080000189

ORIGINAL PAPER

M.R. Barbosa · L.M. Gassa · E.R. Ruiz

Electrochemical behaviour of Ni-Co amorphous alloys in alkaline solutions

Received: 28 December 1998 / Accepted: 29 November 2000 / Published online: 7 June 2001

Abstract The dissolution processes of amorphous G15 ($Ni_{58}Co_{20}B_{12}Si_{10}$) and G16 ($Ni_{25}Co_{50}B_{10}Si_{15}$) alloys in carbonate-bicarbonate buffers ($8.9 \leq pH \leq 10.5$) have been studied using voltammetry and stationary polarization techniques combined with electrochemical impedance spectroscopy and X-ray photoelectron spectroscopy (XPS) measurements. Results indicate that the electrochemical processes are dependent on the applied potential, the alloy composition, and the pH and ionic strength of the electrolyte. An enhancement of the corrosion processes is observed when the pH and the ionic strength are increased and when the Co content of the alloy diminishes. Furthermore, XPS provided information about the composition of the surface layer.

Keywords Ni-Co alloys · Amorphous alloys · Electrochemistry · Electrochemical impedance spectroscopy · X-ray photoelectron spectroscopy

Introduction

The excellent chemical properties of amorphous alloys, as reflected in their mechanical, electrical, catalytic, and magnetic properties, have attracted the attention of many researchers [1, 2, 3, 4]. Certain amorphous alloys show an electrocatalytic activity which is higher than that of their crystalline counterparts and other conventional catalysts. Ni-Co based alloys have been studied extensively owing to their good electrocatalytic properties with respect to the oxygen evolution reaction (OER) in alkaline solutions ([5, 6, 7, 8, 9, 10, 11, 12] and references therein). The use of these materials requires a satisfying resistance to general and localized corrosion. However, it should be noted that neither polycrystalline nor amorphous Ni-Co based alloys have received much attention to establish their dissolution behaviour, as briefly reported in the following.

Linker and Plieth [13] found that the corrosion resistance of Ni-Co glassy metals in both neutral and acid solutions exceeded by about two orders of magnitude those of the corresponding polycrystalline metals. Ball and Payer [14] characterized the corrosion behaviour of different polycrystalline Ni-Co alloys as a function of pH, chloride ion content in the electrolyte, and the alloy composition. Recently, a preliminary corrosion study was carried out on amorphous G15 ($Ni_{58}Co_{20}B_{12}Si_{10}$) and G16 ($Ni_{25}Co_{50}B_{10}Si_{15}$) alloys in carbonate/bicarbonate solutions at pH 8.9 [15, 16]. The results obtained in these investigations showed that the dissolution process of these alloys is markedly dependent on the ionic strength of the electrolyte.

The aim of the present work is to evaluate the influence of pH and ionic strength of slightly alkaline solutions, as well as the alloy composition, on reactions occurring during the dissolution process of G15 and G16 alloys, employing electrochemical techniques combined with X-ray photoelectron spectroscopy (XPS) measurements.

Experimental

G15 and G16 amorphous alloys (Vakuumschmelze, Hanau, Germany) were used as working electrodes. These electrodes were soldered to a copper wire with a conducting epoxy resin as a cold weld (Polytec, Germany); then, the union and the copper wire were enclosed in a glass tube and sealed by an epoxy resin. The seal was completely covered with a Teflon band.

L.M. Gassa (✉) · E.R. Ruiz[1]
Instituto de Investigaciones Fisicoquímicas Teóricas y Aplicadas (INIFTA), Facultad de Ciencias Exactas, Universidad Nacional de La Plata, Sucursal 4, C.C. 16, 1900 La Plata, Argentina
E-mail: lgassa@inifta.unlp.edu.ar

M.R. Barbosa
Facultad de Ingeniería, Universidad Nacional del Centro de la Provincia de Buenos Aires, C.C. 12, 7400 Olavarría, Argentina

Permanent address:
[1]FCEQyN, Universidad Nacional de Misiones

It is known that the electrochemical properties of amorphous alloys are related directly to the fabrication process [4]. For this reason the alloys investigated were produced using the same preparation method (by rapid solidification). The results were obtained employing both shiny and dull sides of the ribbon, with the shiny side situated in front of the Luggin-Haber capillary. Samples were ribbons of 50 μm thickness and 2 cm^2 area. In order to evaluate the influence of Co content on the electrochemical behaviour of glassy metals, electrodes of Vitrovac 0080 ($Ni_{78}B_{14}Si_8$) were used for comparison.

Prior to electrochemical experiments the electrodes were cleaned with analytical grade acetone (Merck), thoroughly rinsed with four-fold distilled water and, finally, cathodically polarized for 30 s in the potential range of the hydrogen evolution reaction (HER), –0.80 V to –1.00 V, in order to provide an electroreduced glassy metal initial surface.

A conventional three-compartment glass cell was used with a large-area Pt counter electrode and a properly shielded calomel reference electrode, which was connected to the rest of the cell through a Luggin-Haber capillary tip. Potentials in the text are referred to the normal hydrogen electrode (NHE) scale.

Electrochemical impedance spectroscopy (EIS) measurements combined with steady-state current-potential curves and single triangular potential sweeps (STPS) between pre-set cathodic ($E_{s,c}$) and anodic ($E_{s,a}$) switching potentials at $v = 0.010$ V s^{-1} were performed under purified N_2 gas saturation in the following solutions at 25°C:

1. 0.75 M $KHCO_3$ + 0.05 M K_2CO_3 pH 8.9 (solution A)
2. 2.50 M $KHCO_3$ + 0.17 M K_2CO_3 pH 8.9 (solution B)
3. 0.75 M $KHCO_3$ + 0.15 M K_2CO_3 pH 9.5 (solution C)
4. 2.50 M $KHCO_3$ + 0.50 M K_2CO_3 pH 9.5 (solution D)
5. 0.75 M $KHCO_3$ + 1.50 M K_2CO_3 pH 10.5 (solution E)

These solutions were prepared with analytical grade (Merck) reagents and four-fold distilled water, which was previously boiled to remove CO_2.

The polarization curves were obtained employing a potentiostat and the potential sweep experiments were carried out using a potentiostat and a function generator (EG&G Parc 173).

Impedance measurements were carried out using a frequency analyser, which included a potenciostat (Zahner IM6d). The experiments were conducted by applying a small amplitude perturbation of 5 mV in a sine waveform, and by scanning the modulus of impedance and the phase shift over the frequency range from 1 mHz to 100 kHz; the applied potential range was $-0.60\ V \le E \le 0.80\ V$.

In addition, XPS measurements were performed using ESCA 3 Mark II equipment, with Mg-K_α X-rays (1 $h\nu = 1253.6$ eV) as excitation source.

Results and discussion

Voltammetric data

For the characterization of the electrochemical behaviour of the amorphous alloys tested in this work, voltammograms were run between the potential regions of the hydrogen and oxygen evolution reactions. The current density/potential (j/E) profiles corresponding to the positive-going potential scan from $E_{s,c} = -0.76$ V to $E_{s,a} = 0.84$ V at $v = 0.01$ V s^{-1} for alloy G15 in the different electrolyte solutions are presented in Fig. 1. The voltammetric profiles of G15 (Fig. 1) show for solutions B–D a first anodic peak (peak I) at about –0.30 V, a second anodic contribution only for solution A (peak II) at ca. 0.05 V, and a third anodic current peak for all solutions (peak III) at ca. 0.70 V. The height of the current peaks was revealed to be dependent on pH, ionic strength, and carbonate-bicarbonate ion concentrations.

The height of current peak I decreases at pH 9.5 as the ionic strength increases (see, for instance, curves C and D). In contrast, the peak I current value increases with ionic strength at pH 8.9. This peak is not observed in solution A, but it is well defined in solutions B–D. In spite of peak I, peak II appears clearly only for solution A, and is not observed for the other solutions. The height of peak III increases when the carbonate concentration increases (see, for instance, the voltammetric response obtained in solutions A, C, and E, and those obtained in solutions B and D) and when the bicarbonate concentration increases, at constant pH (compare curves A with B and C with D).

The voltammograms for alloy G16 (Fig. 2) exhibit during the anodic scan all the current contributions for solution A for alloy G15. However, peak I is only observed in solution A, current peak II is found to be better defined, and peak III appears at more negative potentials for G16 alloy in comparison with G15 alloy.

The voltammperometric response of the pure polycrystalline metals under comparable experimental conditions is well known [17, 18]. Peak I has been associated with Ni to Ni(II) hydroxides active/passive transition [17], peak II was related to the oxidation of Co to oxide-hydroxide species [18], and the third anodic current peak (peak III) corresponds to the redox couple Ni(II)/Ni(III) [17]. The voltammograms of the amorphous metals revealed that the potentiodynamic response could not be interpreted as simple superposition of the typical current peaks corresponding to the single metallic components. Kupka et al. [11] have also shown a mixed voltammetric behaviour for both Ni and Co for an electrodeposited amorphous alloy containing Co, Ni, and P. However, in some cases the overall shapes of the voltammograms reflect the oxide formation of the main metal components; for example, the most intense current peak II in G16 alloy (Fig. 2) can be associated with the high Co concentration of this alloy. Furthermore, the Co

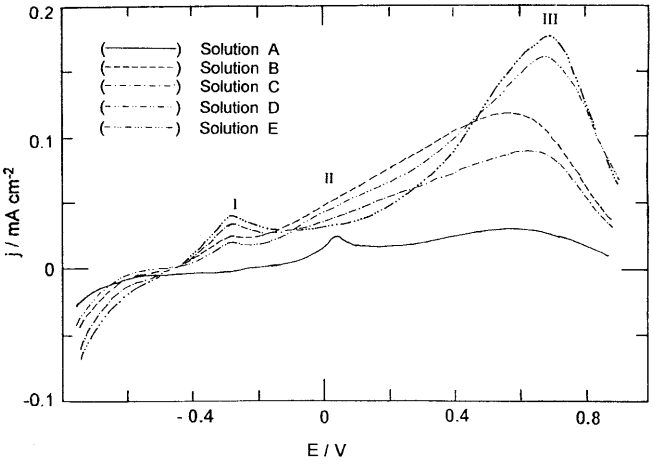

Fig. 1 First positive-going potential scan of alloy G15 in different electrolyte solutions; $v = 0.01$ V s^{-1}

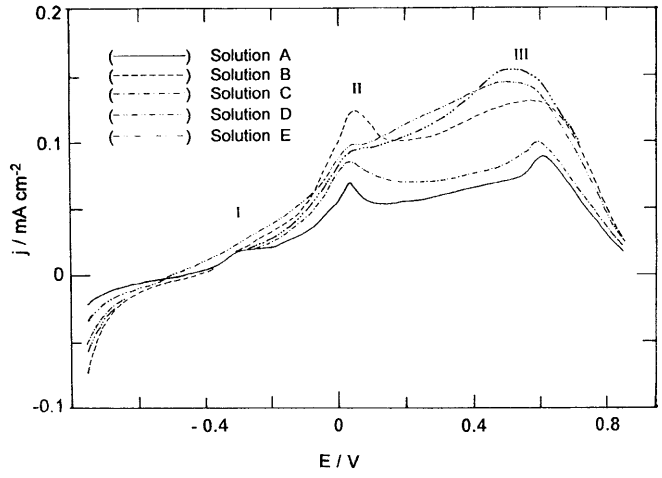

Fig. 2 First positive-going potential scan of alloy G16 in different electrolyte solutions; $v = 0.01$ V s^{-1}

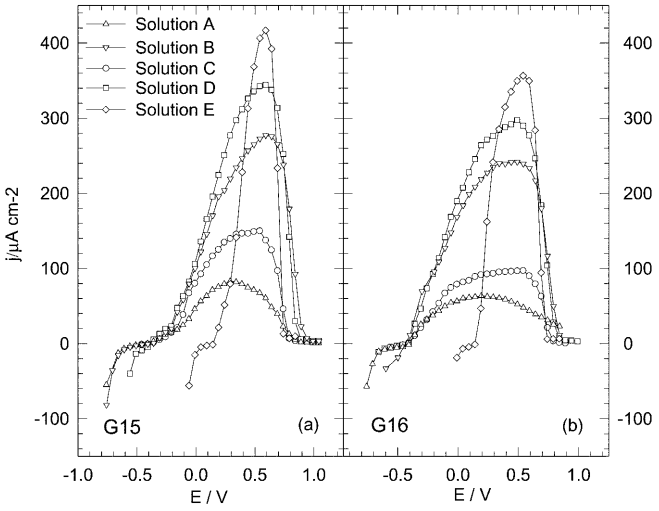

Fig. 3 Stationary polarization curves of alloys **a** G15 and **b** G16 in different electrolyte solutions

influence can be appreciated in the potential shift of peak III (Figs. 1 and 2). These two effects of Co concentration are confirmed with data obtained under similar experimental conditions employing an alloy without Co, such as Vitrovac 0080, in which case, as expected, peak II disappears and peak III shifts to 0.90 V [16]. The Co influence was mentioned also by Lian et al. [10], who suggested that Co additions to $Ni(OH)_2$ stabilize Ni-hydroxide species, improve the conductivity and charge efficiency of $Ni(OH)_2$, and increase the oxygen overpotential. Furthermore, Folquer et al. [19] found in co-precipitated Ni-Co hydroxides a catalytic effect of the Co(II)/Co(III) reaction on the Ni(II)/Ni(III) reaction through hydroxide ions inserted into the metal hydroxide layers.

On the other hand, both Ni and Co hydroxides are hydrous species with an open structure in which Ni(II)/Ni(III) and Co(II)/Co(III) are largely coupled and linked by hydroxide ions inserted into the hydroxide lattice. The hydrous oxides formed on Ni [20] have been described as solvent-filled oxides with potential-pH dependence higher than 60 mV/pH unit. In the case of G15 and G16 alloys, a linear relationship between the peak III potential and pH was considered, and a slope value of ca. 85 mV/pH unit was obtained. This value suggests that the oxidation process of Ni(II) to Ni(III), associated with peak III, involves an excess of OH^- ions in the film formed on the metal surface.

Stationary polarization data

The steady-state polarization curves of alloys G15 and G16 are shown in Fig. 3. A well-defined peak is observed at ca. 0.6 V, probably corresponding to peak III in the voltammetric response. Although the stationary data were obtained under the same initial experimental conditions as those employed in the voltammetric measurements, the contributions of the dissolution processes of Ni and Co (peaks I and II in the voltammograms) are not clearly detected, probably due to the overlapping of peaks I, II, and III. Under the same experimental conditions, this overlapping becomes clearer in the case of the G16 alloy, which presents wider peaks and lower current peak values than G15 alloy in each solution. At constant pH (either solutions A and B or solutions C and D, respectively) the height of the current peaks increases with increasing carbonate concentration of the electrolyte. On the other hand, as the pH increases the current peaks become sharper. It was observed that the current contributions are two or three times higher as the carbonate ion concentration in the solution increased (see, for instance, polarization curves recorded in solutions A, C, and E, as well as those obtained in solutions B and D). The kinetic change observed for the Co-rich alloy supports the idea that the broad peak obtained in steady-state conditions also involves oxidized Co species. The preceding interpretation agrees with a similar change reported for a pure Co electrode in solutions containing carbonate buffer [18].

EIS data

EIS results for the amorphous alloys investigated in this paper are shown in Figs. 4, 5, 6, 7 in the form of Nyquist plots. The Nyquist plots for G15 alloy in solution A (Fig. 4) exhibit, at a potential of $E = -0.36$ V (which is close to the corrosion potential), a capacitive semicircle (Fig. 4a). At increasing positive anodic polarization a superposition of two contributions appears at intermediate frequencies, whereas in the low-frequency region a new capacitive time constant emerges. The latter can be more clearly observed as the operational potential is set more positive (Fig. 4b–d). When the polarization exceeds the peak potential, impedance diagrams reveal a negative resistance component (Fig. 4e, f), in good

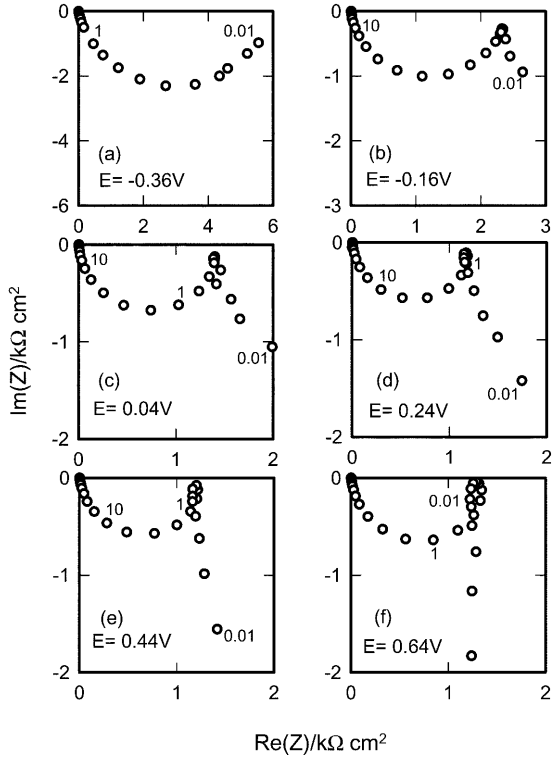

Fig. 4a–f Impedance diagrams for G15 at different applied potentials in solution A (frequencies in Hz)

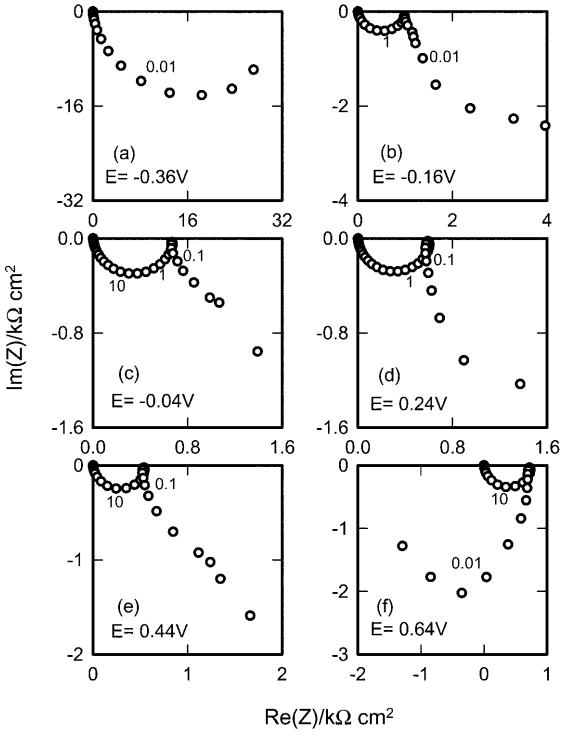

Fig. 5a–f Nyquist diagrams for alloy G16 at different applied potentials in solution B (frequencies in Hz)

agreement with the slope of the steady-state polarization curve.

The frequency responses of G16 alloy in all carbonate/bicarbonate ion containing solutions, covering the 8.9–10.5 pH range, show similar characteristics for the impedance spectra as those for G15 alloy, but involving lower inductance values. The particular case of G16 in solution B, pH 8.9, is shown in Fig. 5a–f.

At constant solution pH and at comparable anodic overpotentials, lower real parts of the impedance and higher inductance values were found as the ionic strength increased [16]. On the other hand, as the pH increased an enhancement of the rate of processes associated with all the time constants was observed (see, for instance, Fig. 6 obtained with G16 alloy in solution D).

The whole set of experimental impedance spectra can be discussed according to the following total transfer function:

$$Z_{\mathrm{T}}(j\omega) = R_{\omega} + Z(j\omega) \tag{1}$$

with:

$$[Z(j\omega)]^{-1} = [\mathrm{CPE}]^{-1} + \left[R_{\mathrm{ct}} + \frac{j\omega L R_{\mathrm{ic}}}{j\omega L + R_{\mathrm{ic}}} + \frac{R_{\mathrm{ad}}}{j\omega C_{\mathrm{ad}} R_{\mathrm{ad}} + 1}\right]^{-1} \tag{2}$$

where R_{Ω} is the electrolyte resistance contribution, $\omega = 2\pi f$, [CPE] denotes the constant phase element given by $[\mathrm{CPE}] = [C_{\mathrm{dl}}\ (j\omega)^{\alpha}]^{-1}$, C_{dl} is the double layer capacitance corresponding to the total (shiny and dull sides) interface electrode/electrolyte. Although the two sides of the electrode appeared different visually, the shiny side and the dull side of the electrode are not involved separately in the model because the electrochemical responses (steady state polarization curves, voltammetry, and EIS) of the both sides of the electrode were similar. This fact was also reported by other authors [21]. The α parameter takes into account the distribution of the time constants due to surface inhomogeneities in amorphous alloys; R_{ct} represents the charge transfer resistance defined as $R_{\mathrm{ct}} = \lim_{\omega \to \infty} \mathrm{Re}[Z]$; L and R_{ic} are associated with the inductive contribution which can be interpreted by assuming a strong potential dependence of the active sites concentration causing surface relaxation phenomena; and R_{ad} and C_{ad} can, in principle, be related to a faradaic pseudo-capacitive contribution of an adsorbed reaction intermediate at the lowest frequencies. The term $\frac{j\omega L R_{\mathrm{ic}}}{(j\omega L + R_{\mathrm{ic}})}$ is necessary to obtain a good fit for the greater part of the experimental impedance response; this fact indicates the presence of a contribution which acts as an inductive loop. When this pseudo-inductive contribution is very small, this term is practically negligible and does not disturb the complete model.

The good agreement between experimental and simulated data according to the transfer function given in the analysis of Eqs. 1 and 2 using non-linear least-square fit routines is demonstrated in Figs. 7 and 8 for alloys G15 and G16 respectively in solutions C and D.

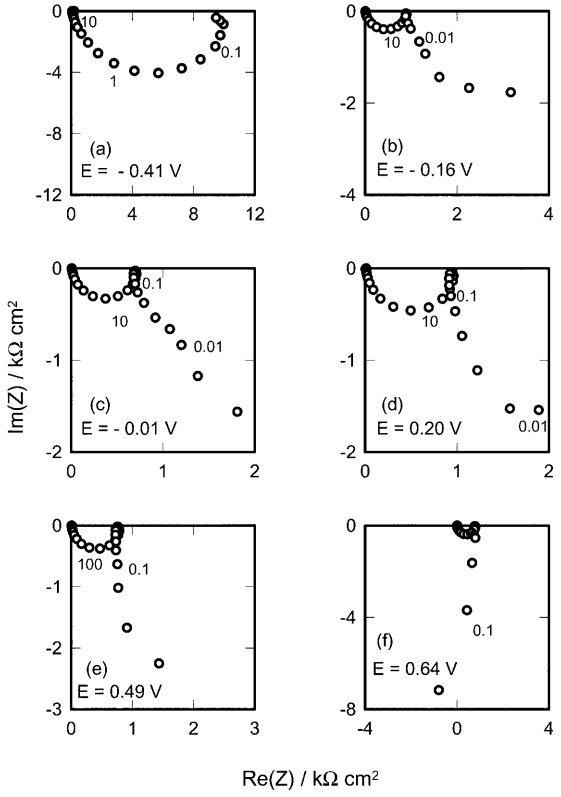

Fig. 6a–f Impedance diagrams for alloy G16 at different applied potentials in solution D (frequencies in Hz)

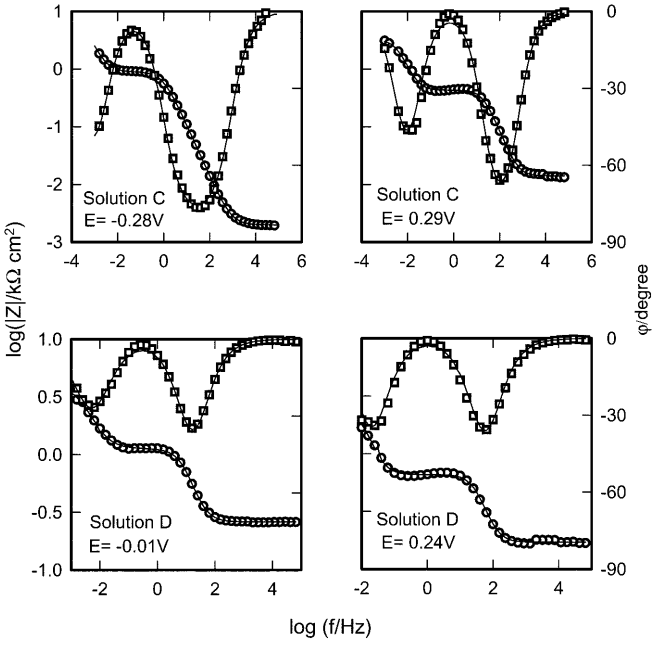

Fig. 7 Experimental $log|Z|$ (○), experimental φ (□), and simulated (–) Bode data diagrams for G15 in solutions C and D

The values of C_{dl} and R_{ct} determined from the optimum fit procedure according to Eqs. 1 and 2, in the potential range $-0.4\ V \le E \le 0\ V$, were

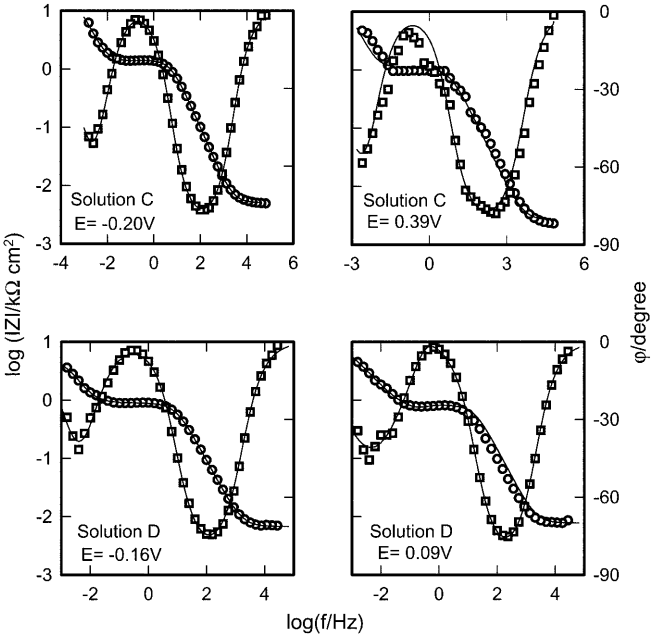

Fig. 8 Comparison of the experimental $log|Z|$ (○), experimental φ (□), and simulated (–) Bode plots for alloy G16 in solutions C and D

$C_{dl} = 30 \pm 10\ \mu F\ cm^{-2}$ and $\alpha = 0.95 \pm 0.05$, while the values of R_{ct} decrease linearly. At positive applied potential the R_{ct} values are nearly constant and lower capacitance values, $C \approx 9 \pm 2\ \mu F\ cm^{-2}$, are obtained. These lower capacitance values are typical of a metal covered with a passive film [22] and may be considered as the passive film and double layer capacitance connected in series. The potential dependence of the capacitance indicates either insulating or semiconducting properties of the passive films. At $E \le 0$ V, $R_{ct} = 0.434b/j_{ss}$ for a charge transfer-controlled reaction, where j_{ss} denotes the steady-state current density and $b = \partial E/\partial \log|j_{ss}|$ is the Tafel slope of the anodic reaction. The calculated value of b was ≈120 mV, which corresponds to a charge transfer coefficient of 0.5.

The analysis of the impedance parameters associated with the time constant contribution at lowest frequencies is difficult because it is a non-complete capacitive loop. However, it was possible to calculate from the fitting an approximate value of $C_{ad} \approx 860 \pm 60\ \mu F/cm^2$.

The fit parameters related to the inductive loop observed at intermediate frequencies fail to obey a direct function of the Ni/Co concentration ratio in the alloy matrix. This is confirmed by the experimental results obtained with Vitrovac 0080, which present an inductive contribution at intermediate frequencies [16].

Furthermore, the criterion of the percentage errors of the parameters determined by non-linear regression was taken into account. In all systems studied the values of the errors were lower than 5% in the case of C_{dl} and R_{ct} and were ≈10% for C_{ad} and R_{ad}. A larger percentage error corresponded to the parameters for the inductive contribution; in this case, the values were 15% and 33% for R_{ic} and L, respectively.

X-ray photoelectron spectroscopy

XPS analysis was carried out to contribute in the identification of species formed during the anodic dissolution of amorphous G15 and G16 alloys.

Figure 9 shows the binding energies obtained at various depths by sputtering with argon for Ni and Co and their related oxides and hydroxides formed on G15 and G16 amorphous alloys after maintaining the specimens under a constant potential corresponding to the main anodic current peak in solution A ($E \approx 0.25$ V).

The surface spectra of G15 and G16 show the signals corresponding to Ni_2O_3 at 856 eV, $Co(OH)_2$ at 781 eV, and CoO at 780 eV [23]. In addition, a low-intensity signal of elemental Ni ($2p_{3/2}$) at 853 eV and elemental Co ($2p_{3/2}$) at 778 eV are observed on G15 and G16, respectively. The depth spectra revealed only the presence of the Ni $2p_{3/2}$ peak for the G15 alloy, while for the G16 alloy the signals corresponding to Ni_2O_3 and $Co(OH)_2$ are observed until a depth of 2 nm. This suggests that the surface layer formed on the Co-rich alloy G16 during the anodic dissolution is thicker than that formed on the G15 alloy. The influence of the average thickness of the mixed oxidized species layers on the dissolution processes of hydrous Ni-Co hydroxide electrodes was reported earlier [19]. Accordingly, the higher anodic currents observed for G15 with respect to G16 in steady-state and EIS measurements should be explained through the formation of a thin layer on the Ni-rich alloy.

The XPS spectra show the presence of silicon for the studied alloys (Fig. 10). On the surface of both alloys it is possible to observe a wide peak at a binding energy of 102–103 eV. These values indicate the presence of silicon oxide and/or silicates whose formation in slightly alkaline electrolyte is probable. Furthermore, it was reported that silicon oxides are the main constituent of the film formed on amorphous alloys with a silicon content as high as 12% [24].

On the other hand, a slight boron oxide signal at 192 eV was detected in the surface and at different depth spectra for both alloys (Fig. 10). It is interesting to note that a signal corresponding to elemental boron is not detected in the surface spectra. Thus, probably the high reactivity of amorphous boron permits the early formation of a boron oxide during the first oxidation steps of the alloys, which remains occluded into the complex film.

It should be noted that the peak for C (not shown here) due to adventitious carbon occurred at about 284.7 ± 0.2 eV in all samples. Therefore, the incorporation of carbonates of cobalt and nickel into the anodic products formed on amorphous alloys can be disregarded, in contrast to that reported elsewhere [17, 18, 25].

XPS spectra obtained in all employed solutions revealed the same general features found in the case of solution A. However, the thicknesses of the surface films formed under identical conditions in more aggressive solutions were found to be much larger.

Some oxides detected by XPS behave as semiconductors and/or dielectrics [26]. This fact agrees with the low capacity values obtained from the EIS measurements.

Conclusions

Electrochemical studies combined with XPS techniques carried out at different polarization potentials yield valuable information about the electrochemical

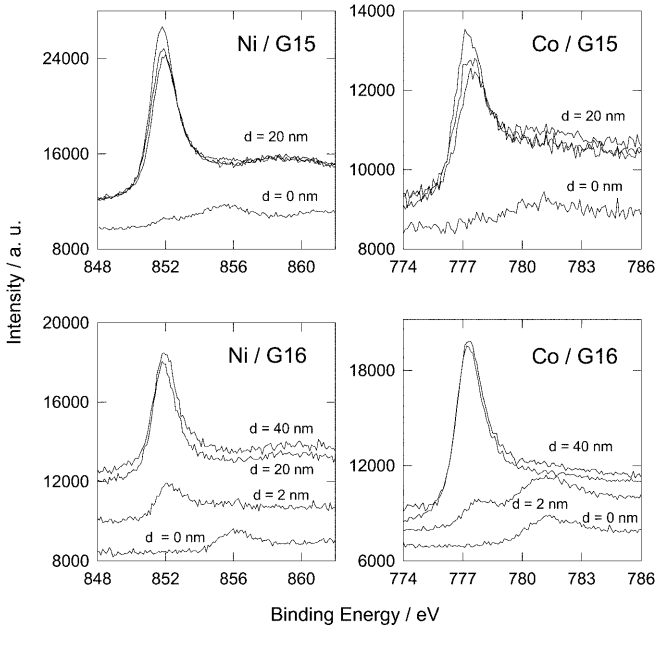

Fig. 9 Ni and Co XPS spectra at different depths corresponding to the alloys G15 and G16 in solution A

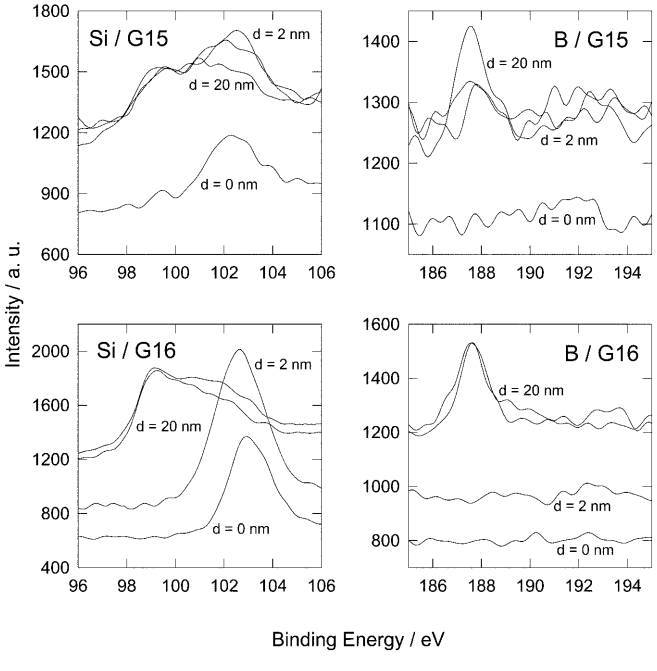

Fig. 10 Si and B XPS spectra at different depths corresponding to the alloys G15 and G16 in solution A

behaviour of amorphous Ni-Co-metalloid alloys in carbonate-bicarbonate buffers, and about the characteristics of the surface species formed. The parameters for the dissolution behaviour of amorphous Ni-Co based alloys were determined as a function of the pH, the ionic strength of the solution, and the alloy composition. The presence of cobalt in the glassy metals leads to considerable lower dissolution rates. An enhancement of the corrosion processes with increasing pH and ionic strength was found. Through XPS measurements the composition of the surface film was determined. Oxide-hydroxide species of the matrix components are found. On the other hand, the thickness of the surface film depends on the electrolyte aggressiveness.

Acknowledgements This research project was financially supported by the Consejo Nacional de Investigaciones Científicas y Técnicas, the Comisión de Investigaciones Científicas de la Provincia de Buenos Aires, the Universidad Nacional de La Plata, the Universidad Nacional del Centro de la Provincia de Buenos Aires, and the Fundación Antorchas. Part of the equipment used in the present work was provided by DAAD and the Alexander von Humboldt-Stiftung.

References

1. Frankenthal RP, Kruger J (eds) (1978) Passivity of metals. The Electrochemical Society, Princeton
2. Froment M (ed) (1983) Passivity of metals and semiconductors. Elsevier, Amsterdam
3. Diegle RB, Hashimoto K (eds) (1988) Corrosion, electrochemistry and catalysis of metallic glasses. The Electrochemical Society, Pennington
4. Searson PC, Nagarkar PV, Latanision RM (1990) Electrochemistry of metallic glasses. In: White RE, Bockris JO'M, Conway BE (eds) Modern aspects of electrochemistry, vol 29. Plenum Press, New York, pp 121–161
5. Kreysa G, Hakansson B (1986) J Electroanal Chem 201:61
6. Alemu H, Jüttner K (1988) Electrochim Acta 33:1011
7. Kessler T, Vilche JR, Ebert M, Jüttner K, Lorenz WJ (1991) Chem Eng Technol 14:263
8. Lian K, Kirk DW, Thorpe SJ (1991) Electrochim Acta 36:537
9. Lian K, Thorpe SJ, Kirk DW (1992) Electrochim Acta 37:169
10. Lian K, Thorpe SJ, Kirk DW (1992) Electrochim Acta 37:2029
11. Kupka J, Budniok A (1990) J Appl Electrochem 20:1015
12. Lian K, Kirk DW, Thorpe SJ (1995) J Electrochem Soc 142:3704
13. Linker U, Plieth WJ (1985) Investigation of the role of boron and nickel for the corrosion behaviour of metallic glasses. In: Steeb S, Warlimont H (eds) Rapidly quenched metals. Elsevier, Amsterdam, pp 1465–1468
14. Ball GR, Payer JH (1993) In: Gundry RD (ed) Proceedings of the 12th international corrosion congress. NACE, Houston, pp 1132–1142
15. Gassa LM, Vilche JR, Barbosa MR (1995) Mater Sci Forum 192–194:825
16. Barbosa MR, Gassa LM (1997) J Braz Chem Soc 8:143
17. Bohé AE, Vilche JR, Arvia AJ (1990) J Appl Electrochem 20:418
18. Gervasi CA, Biaggio SR, Vilche JR, Arvia AJ (1989) Corros Sci 29:427
19. Folquer ME, Vilche JR, Arvia AJ (1984) J Electroanal Chem 172:235
20. Burke LD, Twomey TAM (1984) J Electroanal Chem 167:285
21. Lian K, Birss VI (1991) J Electrochem Soc 138:2877–2884
22. Simões AMP, Ferreira MGS, Rondot B, da Cunha Belo M (1990) J Electrochem Soc 137:82
23. Moulder JF, Stickle WF, Sobol PE, Bomben KD (1995) Data interpretation. In: Chastain J, King RC Jr (eds) Handbook of X-ray photoelectron spectroscopy. Physical Electronics, Eden Prairie, Minn., pp 16–85
24. Janik-Czachor M (1985) J Electrochem Soc 132:306
25. Gassa LM, Barbosa MR, Real SG, Vilche JR (1995) Corros Sci 37:1115
26. Morrison SR (1984) Electrochemistry at semiconductor and oxidized metal electrodes. Plenum Press, New York